Clays and Clay Minerals, Vol. 39, No. 4, 437–445, 1991.

DETECTION OF TRACE AMOUNTS OF ERIONITE USING X-RAY POWDER DIFFRACTION: ERIONITE IN TUFFS OF YUCCA MOUNTAIN, NEVADA, AND CENTRAL TURKEY

DAVID L. BISH AND STEVE J. CHIPERA

Earth and Environmental Sciences Division, Los Alamos National Laboratory
Los Alamos, New Mexico 87545

Abstract—Recent data in the biological literature suggest that the natural zeolite erionite may be more tumorigenic than asbestos minerals. Because of its potential biological importance, a technique has been developed to facilitate detection of erionite in tuffaceous rocks to a lower limit of detection (LLD) between 100 and 500 ppm. The method involves the use of automated X-ray powder diffraction instrumentation with long count times, as much as 360 s/step. The presence of interfering phases, such as smectite or clinoptilolite, raises the LLD. Ethylene glycol solvation of smectite improves the LLD, and profile fitting with clinoptilolite-bearing mixtures improves quantification. Application of these methods to tuffs from central Turkey allowed improved detection and more accurate quantification compared with previous scanning electron microscope examinations. Use of these methods with tuffs from Yucca Mountain, Nevada, the potential site for the nation's first high-level radioactive waste repository, showed that erionite occurs sporadically. Erionite is found only in the altered zone directly above the lower vitrophyre of the Topopah Spring Member. This altered zone is anomalous in that is contains a variety of zeolites that are either rare or absent in other Yucca Mountain tuffs. It appears that erionite is restricted to fractures and must have formed under unusual and variable conditions in the altered zone.

Key Words—Clinoptilolite, Detection limits, Erionite, Profile refinement, X-ray powder diffraction, Zeolitic tuffs.

INTRODUCTION

The fibrous zeolite erionite is relatively common in zeolite deposits throughout the world. It was first discovered in large amounts in sedimentary deposits by Deffeyes (1959) and has since been documented in numerous localities and geologic environments. Before the 1970s, erionite was viewed as a useful zeolite with high stability in the dehydrated form. Erionite has received considerable commercial attention as a shape-selective component in cracking catalysts. However, reports emerged in the 1970s about a potential connection between the occurrence of erionite in south-central Turkey and high incidences of pleural mesothelioma in the two villages, Karain and Tuzköy (e.g., Bariş *et al.*, 1975). Mumpton (1979) summarized the research, mostly by medical workers, that led to the conclusion that erionite was the cause of mesothelioma in the village inhabitants of central Turkey. He showed that although erionite is found in the villages where pleural mesothelioma occurs, it also occurs in villages such as Sarihidir with initially no reported cases of mesothelioma. This suggested that some other agent may be responsible for the high incidence of mesothelioma. More recent reports, however, have shown that mesothelioma also occurs at unusually high rates in Sarihidir (Bariş *et al.*, 1987; Simonato *et al.*, 1989). Because of the apparent deleterious health effects of erionite, this common natural zeolite has understandably recently received considerable attention from researchers not traditionally concerned with zeolites.

The biological importance of erionite led us to begin an investigation of the distribution of erionite in the tuffaceous rocks at Yucca Mountain, Nevada, the potential site for the nation's first high-level radioactive waste repository. Yucca Mountain is located in southwestern Nevada and consists of a sequence of ash-flow and air-fall tuffs, ranging from nonwelded to densely welded. Many of the nonwelded units are pervasively zeolitized. The mineralogy of the rocks at Yucca Mountain was documented by Broxton *et al.* (1987) and Bish and Chipera (1989a). The welded crystalline rocks consist primarily of variable amounts of alkali feldspars, quartz, cristobalite, tridymite, and minor amounts of smectite. The nonwelded rocks range from almost completely vitric (glassy) to fully altered rocks containing variable amounts of clinoptilolite, mordenite, alkali feldspar, quartz, opal-CT, and minor smectite. A vitrophyre (densely-welded glassy unit) occurs near the bottom of the Topopah Spring Member of the Paintbrush Tuff, the unit proposed as the host rock for the potential repository. The vitrophyre is composed of glassy material with minor amounts of alkali feldspar and quartz. Carlos (1985) showed that mordenite and other authigenic minerals occur in fractures of the devitrified Topopah Spring Member of the Paintbrush Tuff. A petrologically complex zone, 10- to 20-m thick, directly overlies this vitrophyre and consists of a va-

riety of alteration minerals, including smectite, clinoptilolite/heulandite, quartz, alkali feldspar, and sporadic occurrences of other zeolites such as erionite, mordenite, chabazite, and phillipsite.

In addition to the Yucca Mountain samples examined, several samples of tuffaceous material from Karain, Turkey, and surrounding villages were supplied by F. A. Mumpton. The samples were examined to test methods designed to detect low concentrations of erionite, and to compare the X-ray diffraction results with previous scanning electron microscopy results.

Biological effects of erionite

An ever-increasing body of literature is available showing the apparent significant biological effects of erionite. After the initial reports of the link between erionite and mesothelioma in Karain, Turkey, Rohl *et al.* (1982) reexamined lung tissue and rock samples from the region in south-central Turkey. Significant amounts of tremolite and chrysotile were reported in addition to erionite in both environmental and lung tissue samples. They concluded that their findings were consistent with published data showing a relationship between *asbestos* (chrysotile or amphibole) exposure and pleural disease, and they speculated on the existence of an enhanced tumorigenic effect produced by a combination of asbestos and erionite. Sèbastien *et al.* (1984) also concluded that the high frequency of mesothelioma in the central Turkish villages was related to airborne exposure to natural mineral fibers.

Wagner *et al.* (1985) examined the relationship between erionite exposure and mesothelioma through experimental studies on rats. They found that samples of erionite from Turkey and Oregon produced a very high incidence of mesothelioma and remarked that no other dusts they had investigated (including asbestos) produced such a high incidence of tumors. Suzuki and Kohyama (1988) studied the effects of intraperitoneal administration of mordenite and two natural erionites in mice. (The peritoneum is the membrane lining the walls of the abdominal cavity.) They found that both erionites produced malignant peritoneal tumors at a high rate, but mordenite produced no tumors. Coffin *et al.* (1989a,b) and Palekar *et al.* (1989) also obtained both *in vitro* and *in vivo* results demonstrating that erionite is much more tumorigenic than crocidolite or chrysotile and induces chromosomal abnormalities. In one of the few studies on mechanisms of tumorigenesis, Coffin *et al.* (1989a) sought to explain why erionite is more tumorigenic than either crocidolite or chrysotile, in spite of the fact that the latter two minerals typically have a far greater percentage of fibers in the length-to-width class considered dangerous. They invoked the high internal surface area of erionite (~200 m^2/g) compared with the total surface areas for chrysotile and crocidolite (~24 m^2/g and 8–10 m^2/g, respectively) as a possible reason for the observed differences in tumorigenesis. Interestingly, they found that encapsulation of isopentane in the internal structural cavities of erionite reduced the cytotoxicity, and exchange with Ca^{2+} increased the cytotoxicity of erionite in *in vitro* studies with hamster lung cells.

Detection limits for X-ray powder diffraction analyses

From previous investigations of Yucca Mountain samples it was clear that erionite, if present, would exist only in trace amounts. In addition to the complicating effects of very low erionite concentrations, mordenite in the Yucca Mountain rocks can be mistaken for erionite in the optical or scanning electron microscope (SEM), and the compositional similarities between erionite and other zeolites in the rocks make precise identification based on chemical composition difficult. Although the Si/Al ratio is higher for mordenite than for erionite, the semi-quantitative nature of most SEM chemical analyses hinders exact identification. In our experience, only diffraction methods (e.g., X-ray or electron diffraction) provide unequivocal identification of erionite.

In the report of a reconnaissance study on zeolites in central Turkey, Mumpton (1979, p. 44) stated the commonly held conception at that time regarding detection limits using X-ray powder diffraction methods on geological samples. "Inasmuch as X-ray powder diffraction, even under the best of conditions, is incapable of detecting zeolite minerals at levels less than about 1%, it is vital that all samples be examined by careful electron microscopy, utilizing both scanning and transmission techniques and selected-area diffraction where possible." Before beginning our analyses, it was necessary to examine critically the common conception regarding detection limits in the mineralogical field and to determine the effects of sample- and instrument-related parameters on detection limits for erionite in zeolitic tuffs.

Few analysts determine detection limits when performing quantitative analysis by X-ray powder diffraction, and when quoted, these limits vary widely. Klug and Alexander (1974) briefly mentioned detection limits and quoted values of minimum detection limits ranging upwards from 2% for quartz, kaolinite, and montmorillonite in a noncrystalline matrix. Carter *et al.* (1987) analyzed beneficiated bentonites for quartz and cristobalite using a combined internal standard/mass absorption coefficient correction method. They estimated the minimum detection limits to be 0.001% for quartz and 0.003% for cristobalite, and chose figures ten times these values as the lower limit of quantification. In a study of the ability of X-ray powder diffraction methods to detect small amounts of asbestiform minerals, Puledda and Marconi (1989) used lightly-loaded silver filters and a correction for X-ray absorption to analyze amphibole samples. Analyses of

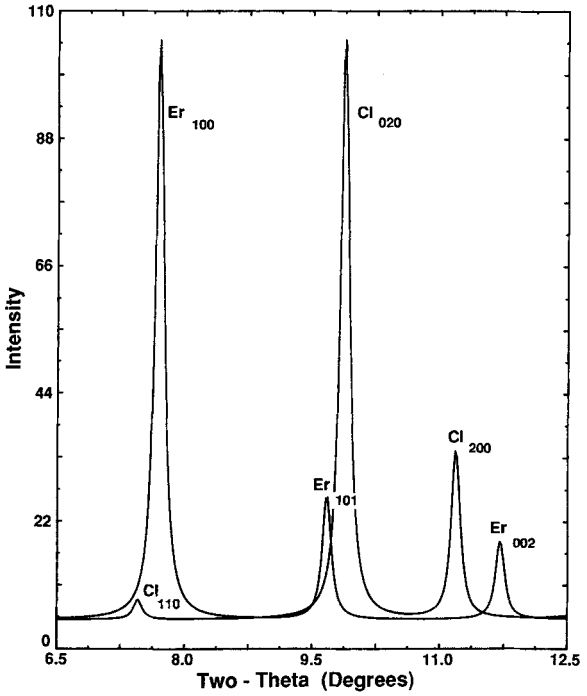

Figure 1. Diffraction patterns of clinoptilolite (Cl) and erionite (Er). CuKα radiation, calculated with POWD10 (Smith *et al.*, 1982). Patterns were calculated separately and then superimposed, with the erionite 100 reflection and the clinoptilolite 020 reflection each assigned a relative intensity of 100. Note the overlap between the clinoptilolite 110 reflection at ~7.48°2θ and the erionite 100 reflection at ~7.67°2θ.

various pure amphibole asbestos minerals yielded detection limits ranging from 2.2 μg for tremolite to 8.4 μg for anthophyllite. Detection limits for crocidolite in three different noninterfering matrices were ~5 μg. Clearly, X-ray powder diffraction methods are capable of detecting very small amounts of crystalline materials.

Implicit in all discussions of minimum detection limits is the fact that the limits are a function of both instrumental (e.g., count times, scan rates, types of slits, and tube power) and sample-related (e.g., scattering power, overlapping reflections) parameters. Chung (1974) formalized the relationship between background count rate, absolute scattering power of a particular reflection for a given phase, and the detection limit. Davis (1988) also outlined the procedure for estimating detection limits in quantitative analysis by X-ray powder diffraction using the reference intensity method. Generally, a peak is considered observed if it is at least three times the standard deviation (σ_b) of the background intensity at a given 2θ position (99% confidence limit; some authors use 2σ_b, i.e., 95% confidence limit), where the standard deviation of background intensity is the square root of the background counts accumulated in t seconds (C_b). The lower limit of detection (LLD) in intensity is then 3σ_b or 3$\sqrt{C_b}$. Thus, although background counts, C_b, increase linearly with count time, σ_b increases as the square root of C_b. From this relationship, it is obvious that a straightforward way to reduce the minimum detection limit is either to increase the count time at each step in a pattern or decrease the scan rate.

Detection by X-ray powder diffraction of trace amounts of erionite in zeolitic rocks is hindered by its coexistence with smectite and clinoptilolite. Even a relatively weak, broad, and diffuse smectite 001 reflection can mask the presence of trace erionite. In addition, the clinoptilolite 110 reflection near 7.48°2θ (CuKα) can easily mask the 100 erionite reflection near 7.67°2θ if clinoptilolite is present in significant amounts (Figure 1). In fact, some mineralogists mistakenly have identified the presence of small amounts of erionite in clinoptilolite-bearing rocks based solely on a reflection near 7.5°2θ (F. A. Mumpton, personal communication). The X-ray powder diffraction pattern for clinoptilolite in the JCPDS file does not indicate the existence of the clinoptilolite 110 reflection, whereas all our observed and calculated patterns of clinoptilolite clearly show this low-angle reflection, with a calculated intensity of ~3 (see Figure 1). Observed intensities of this reflection in our measured patterns of seven clinoptilolites range from 1 to ~4. In addition, neither of the two observed heulandite patterns in the JCPDS shows the 110 reflection, although the calculated heulandite pattern (25–144) includes this reflection with a relative intensity of 6.

In the present studies, the instrumental and sample parameters required to optimize detection of erionite in bulk zeolitic samples by X-ray powder diffraction were determined first. A number of standard zeolites mixed in known proportions, and a variety of natural zeolite samples were examined before studying samples from either Yucca Mountain drill holes or central Turkey.

EXPERIMENTAL METHODS

Reference erionite specimens collected by the authors and purchased from Minerals Research, Clarkson, New York (sample numbers in parentheses), included samples from Pine Valley, Nevada (27094); Needle Peak, Nevada (25216); Wikieup, Arizona (25218); Shoshone, California (25219); and Eastgate, Nevada (25220). Erionite samples collected from Kirkland Junction, Arizona; Rome, Oregon; and Bowie, Arizona were also used. In our investigations erionite 27094 was used as a primary standard. Other reference zeolites were also examined, including analcime from Wikieup, Arizona (25608), and clinoptilolite samples from Agoura, California; Buckhorn, New Mexico (27083); Castle Creek, Idaho (27032); Death Valley Junction, California (27163); Fish Creek Mountains, Nevada (27054); Horseshoe Dam, Arizona; Mountain

https://doi.org/10.1346/CCMN.1991.0390413 Published online by Cambridge University Press

Green, Utah (27063); Vulture Creek, South Africa; and Sheaville, Oregon (27073).

Several samples from central Turkey (provided by F. A. Mumpton, his numbers 26-74-61, 62, 63; 26-74-76, and 26-74-95) also were examined to compare with earlier analyses for erionite. The first three samples are from bedrock near houses and caves in the village of Karain. According to Mumpton, they are all volcanic ash with a trace of K-feldspar, cristobalite, and albite. A trace of erionite was identified in these three samples using the SEM. Sample 26-74-76 from Karlik, Turkey, is of a wall block containing predominantly cristobalite and K-feldspar, with traces of quartz, erionite, and montmorillonite. SEM examination of this sample suggested an erionite content of 5–10%. Sample 26-74-95 from the village of Uçhisar, is of bedrock and consisted predominantly of vitric ash with small amounts of albite, K-feldspar, illite, and cristobalite. SEM examination did not reveal the presence of erionite.

Prior to preparation of mixtures, all samples were ground under acetone to an average particle size of <3 μm in a Brinkmann Micro-Rapid Mill. Particle-size distributions were verified using a Horiba Centrifugal Particle Size analyzer calibrated using Duke Scientific glass microanalysis spheres. Using erionite 27094, mixtures with purified clinoptilolite 27054 were prepared containing 0.05–20.0% erionite. Diffraction patterns of the 0.05–1.0% mixtures are shown in Figure 2. The mixtures were prepared by weighing appropriate amounts of the two minerals and mixing and homogenizing them under acetone in a Brinkmann Micro-Rapid Mill with an agate mortar and pestle. Mixtures from 0.5–20% were prepared to total 2.0 g, and those from 0.05–0.25% totaled 4.0 g. All weighings used a Mettler AE-50 balance annually calibrated with standards traceable to the National Institute of Standards and Technology (NIST). Mixtures containing $<0.05\%$ (500 ppm) erionite were not prepared due to uncertainties involved in weighing and homogenizing very small amounts of erionite with large amounts of clinoptilolite. Several mixtures made using clinoptilolite 27032 and the Rome erionite yielded similar results for detection limits. In addition, a mixture was prepared with 0.05% erionite 25218 and 99.95% analcime 25608 as an example of a mixture without erionite peak interference.

The effectiveness of homogenization was evaluated by examining the 99:1 and 99.9:0.1 clinoptilolite : erionite mixtures. X-ray diffraction analysis of six different mounts of each of these two mixtures revealed variations from mount to mount no larger than the uncertainty due to counting statistics. Thus, sample homogenization did not appear to be a problem. A simplified analysis of the 4-g mixture containing 0.05% erionite (assuming a density of clinoptilolite and erionite of 2.15 g/cm^3 and cubic crystals 3 μm on a side) shows that the mixture will contain 6.9×10^{10} clinoptilolite crystallites and 3.4×10^7 erionite crystallites. Thus, although the ratio of erionite to clinoptilolite is small in the low-erionite mixtures, these mixtures still contain millions of erionite crystallites.

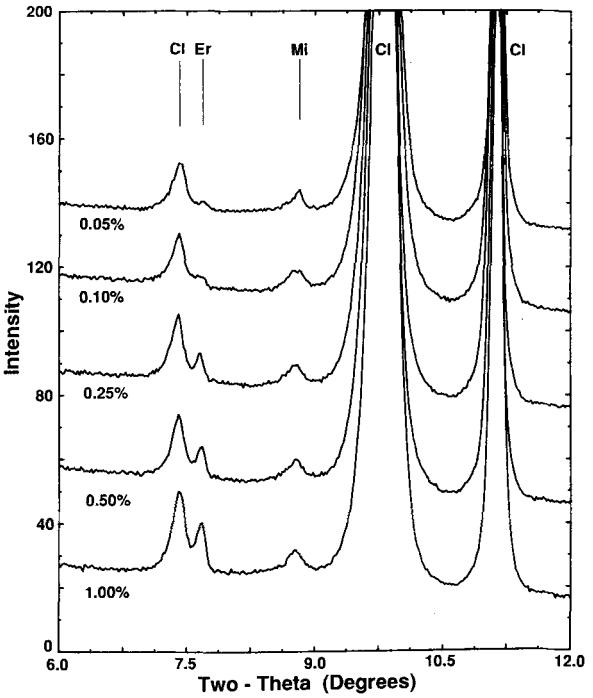

Figure 2. Diffraction patterns of different proportions of 27054 clinoptilolite and 27094 erionite, CuKα radiation, Cl = clinoptilolite, Er = erionite, Mi = mica. Erionite proportions (0.05–1.00%) are shown beneath the respective diffraction patterns.

Most powdered samples (≤ 3 μm) were mounted in a cavity in a solid aluminum block, but smectite-bearing samples and those for which little sample was available were mounted as water smears on an off-axis cut ("zero-background") quartz plate. The water smears yielded greater preferred orientation than the cavity mounts (see below). Concentration effects due to differential settling in these thin mounts are unlikely because the mounts were not infinitely thick and the complete powder was sampled by the X-rays. Because of transparency effects with the water-smear mounts, they were used only for detection and not for quantification. Water-smear mounts were glycolated to shift any smectite reflections to lower 2θ values, thus reducing the smectite overlap on the erionite 100 reflection. The glycolated mounts were X-rayed in an ethylene glycol-saturated atmosphere using an enclosed sample cell fitted with X-ray transparent windows. Some samples, including several ethylene glycol-solvated samples, were examined on the diffractometer in a helium atmosphere to minimize the effects of low-angle air scatter. This treatment had the effect of further reducing the background at the position of the erionite 100 reflec-

https://doi.org/10.1346/CCMN.1991.0390413 Published online by Cambridge University Press

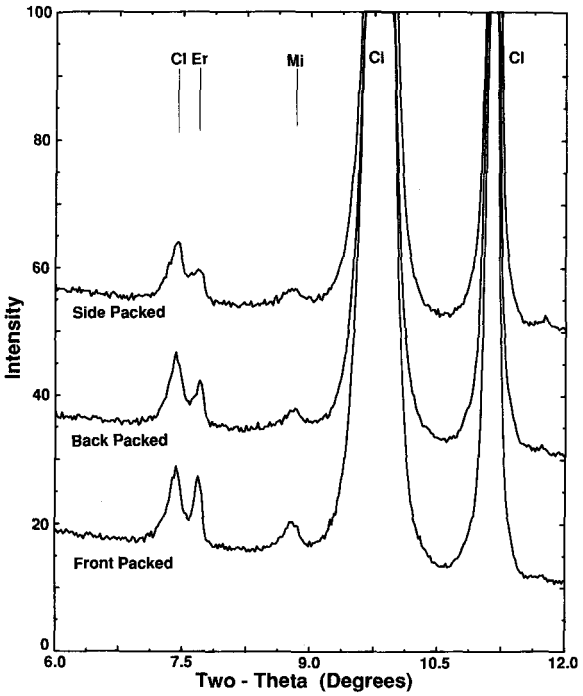

Figure 3. Diffraction patterns of a 01:99 erionite-clinoptilolite mixture using three sample mounting techniques (abbreviations as in Figure 2).

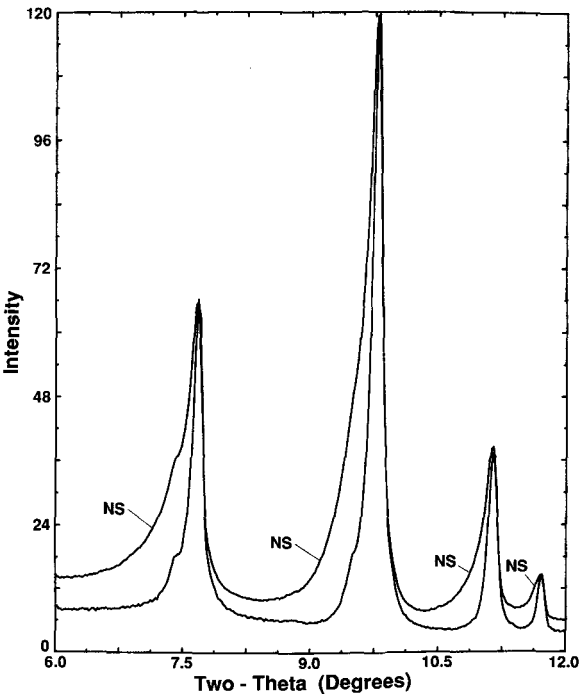

Figure 4. Effects of Soller slits on peak shapes at low angles from an erionite and clinoptilolite mixture. The pattern labeled "NS" was obtained without incident-beam Soller slits, and the lower unlabeled pattern was obtained with incident-beam Soller slits.

tion. Although it is generally desirable to minimize preferred orientation of crystallites in a powder-diffraction sample mount, the preferred orientation occurring with the water-smear mounts actually improved the detection limits for erionite by enhancing the erionite 100 reflection. Figure 3 shows the diffraction patterns for a 99:0.1 mixture of clinoptilolite : erionite using three sample mounting techniques. Note that the erionite 100 reflection at ~7.67°2θ is enhanced in the pattern obtained from the front-packed mount as compared with the patterns obtained with back- or side-packed mounts.

X-ray powder diffraction (XRD) analyses were performed on an automated Siemens D-500 diffractometer employing CuKα radiation, a graphite diffracted-beam monochromator, and incident- and diffracted-beam Soller slits. The use of both incident- and diffracted-beam Soller slits was crucial in reducing the low-angle broadening of reflections due to axial divergence of the X-ray beam. Their use improved both the detection of weak erionite reflections at low 2θ angles and the discrimination between the erionite 100 and the clinoptilolite 110 reflection (Figure 4). Towards the end of this study, diffraction patterns were obtained using a Kevex Psi solid-state Si detector. This yielded at least a factor of three increase in count rate over the scintillation detector/monochromator system due primarily to the elimination of the graphite monochromator (Bish and Chipera, 1989b). All sample mounts were long enough to accept the X-ray beam fully at the lowest angle of interest, ~6°2θ. Routine reconnaissance data for all samples were collected from 2°–36°2θ, counting for 2.0 s every 0.02°2θ step. Data collection for the detection of trace erionite involved scanning from 6°–9°2θ, counting for at least 120 s every 0.02°2θ. Although the count times involved are unusually long, these data collection parameters posed no operational difficulty as each measurement was accomplished overnight, with a few experimental runs conducted over weekends. The long-term stability of our X-ray generator was evaluated by making 50 repetitive measurements over the region of the quartz 100 reflection for a three-day period. The mean maximum intensity for this reflection was 4062 ± 16.3 (1σ) counts, and the mean integrated intensity was 484.3 ± 2.2 (1σ) counts. There was no detectable long-term drift in intensities.

Peak positions and integrated intensities were measured using the Siemens DIFFRAC 5000 first-derivative peak-search routine. NIST SRM 640b silicon was used to calibrate the instrument. Profile refinement of the low-angle reflections was performed with the Siemens DIFFRAC 5000 FIT program using a split Pearson VII profile. External standard quantitative analyses were performed for all samples using an er-

https://doi.org/10.1346/CCMN.1991.0390413 Published online by Cambridge University Press

ionite reference intensity ratio (RIR) value of 1.0, and internal standard analyses were done for most samples using an addition of 20% (by wt.) 1.0-μm corundum. The RIR is defined as the ratio of the integrated intensity of a given reflection of the phase of interest to the integrated intensity of the 113 reflection of corundum in a 1:1 mixture by weight. All analyses for noncrystalline material were obtained by the difference from 100% using the internal standard method (Chung, 1974).

To quantify the variations in the position of the erionite 100 reflection for differentiation from the clinoptilolite 110 reflection, accurate positions were determined for this reflection using the erionite reference samples. Results for seven samples gave an average position of 7.67 ± 0.03°2θ (1σ) (CuKα). Bish (1984) quoted an average position for the clinoptilolite 110 reflection (n = 11) of 7.48 ± 0.04°2θ (1σ), significantly different from the erionite 100 position.

After development and testing of a measurement technique to optimize erionite detection, we examined the above reference samples, 76 bulk rock and 12 fracture samples from drill cores obtained at Yucca Mountain, Nevada, and the samples from Turkey. A list of the Yucca Mountain samples and their locations and bulk mineralogy were reported in Chipera and Bish (1989). Additional samples from Yucca Mountain have subsequently been examined.

RESULTS AND DISCUSSION

Detection limits

The detection limits for erionite varied considerably depending on the matrix within which the erionite occurred, on the particular erionite used, and on the data-collection parameters used. The lowest detection limits were obtained for samples containing no interfering reflections from other phases, such as clinoptilolite or smectite. For example, the calculated LLD for erionite in analcime using a count time of 256 s/step with the Kevex Psi detector was ~120 ppm (Figure 5).

The most reproducible quantitative results for samples containing both erionite and clinoptilolite were obtained when the individual erionite and clinoptilolite reflections were profile fit. This method allows decomposition of overlapping reflections and accurate apportionment of intensities between two or more reflections. Because the erionite 100 reflection overlaps significantly with the clinoptilolite 110 reflection, accurate measurement of intensities at low erionite concentrations is difficult without profile refinement. Using the prepared mixtures of clinoptilolite and erionite and conventional scanning parameters (0.02°2θ steps, 2.0 s/step), erionite could be readily detected in concentrations as low at 0.25 wt. %. Using the long count-time methods described above and profile fitting, the LLD for erionite in clinoptilolite-bearing samples was

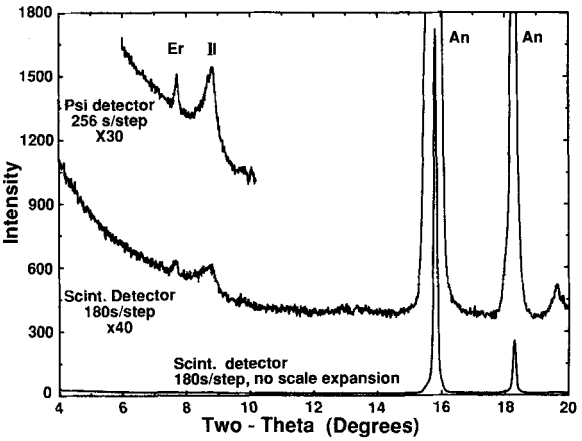

Figure 5. Diffraction pattern of 0.05% erionite in analcime. Lower pattern has the most intense analcime reflection on scale, whereas the central pattern has been scaled up by a factor of 40. The upper pattern was obtained with the Psi detector counting for 256 s/step and has been scaled up by a factor of 30. The reflection at ~8.8°2θ is due to illite (Er = erionite, Il = illite, An = analcime).

~250 ppm for Pine Valley erionite (180 s/step count time), ~500 ppm for Needle Peak erionite, and ~750 ppm for Rome erionite (750 s/step). Increasing the count time per step to 999 s reduced the LLD for Pine Valley erionite to ~150 ppm.

Smectite in a sample adversely affected the ability to detect small quantities of erionite due to overlap of the broad smectite 001 reflection on the erionite 100 reflection. However, Figure 6 shows that solvation of the smectite with ethylene glycol shifts the smectite 001 reflection to lower angles sufficiently to reduce extraneous intensity at ~7.5°2θ, thus improving detection limits. Detection limits for erionite in smectite-bearing samples, using the prescribed counting methods and ethylene glycol-solvated samples, are ~500 ppm and comparable to those for clinoptilolite-bearing samples. Mixtures of erionite with interstratified illite/smectite (I/S) may not be amenable to the procedure using ethylene glycol if the I/S 001 reflection does not shift to ~16.9 Å.

All quantitative analyses reported here used the reference intensity methods of Chung (1974). Reference intensity ratios were measured for erionite using mixtures of erionite and metallurgical-grade 1.0-μm corundum. Values obtained for the erionite 100 reflection were 0.77 ± 0.06, 0.96 ± 0.03, and 1.43 ± 0.07 for the Rome, Needle Peak, and Pine Valley erionites, respectively. All RIR values were obtained using front-pack mounts, integrated intensities, and are the mean of six independent measurements. Errors are 1σ values. The variation between these RIR values is attributed primarily to preferred orientation due to variations in morphology, although chemical effects may also be important. These values compare with

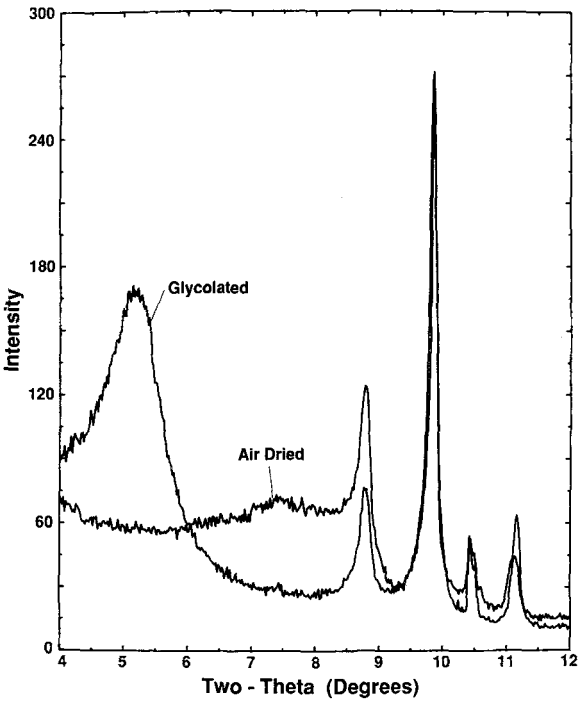

Figure 6. Effects of ethylene-glycol solvation on a smectite-zeolite diffraction pattern (sample contains no erionite). Note the significant reduction in intensity near the position of the erionite 100 reflection at ~7.67°2θ, whereas the clinoptilolite reflections at ~9.8°2θ in the two patterns overlap closely.

mean measured values of 0.91, 1.80, and 4.19 for the strongest reflections of clinoptilolite, analcime, and quartz, respectively. Because these values are a measure of how strongly an individual mineral diffracts X-rays, erionite detection limits are obviously comparable to those for clinoptilolite, but much worse than those for quartz.

Erionite analyses

Turkish samples. The five Turkish samples examined with the internal standard method were composed primarily of noncrystalline volcanic ash (58–95%), with varying amounts of smectite, quartz, feldspar, mica, cristobalite, calcite, chlorite, and hornblende. Samples 61 and 62 contained halite, a phase not reported by Mumpton (1979). Otherwise, these bulk mineralogical results compare reasonably well with his results. All five samples examined showed a reflection of varying intensity at 7.71–7.74°2θ, showing that all samples contained erionite. Samples 61, 62 and 95 contained ~0.2% erionite, several times the LLD, and sample 63 contained erionite near the LLD. Sample 76 contained 2.3 ± 1% erionite, somewhat less than the 5–10% estimated by Mumpton using the SEM.

These results show the diverse nature of these samples and emphasize the importance of obtaining accurate quantitative mineralogical information on samples of biological importance. For example, sample 26-74-95 contains detectable erionite although previous SEM examination did not reveal the presence of any fibrous material. Considering the treatment of other fibrous materials by the biological community (e.g., the belief by some that only one asbestos fiber may be dangerous), it is probable that the level of erionite in this sample would be deemed significant by some workers. The X-ray diffraction results also illustrate the difficulty in obtaining accurate quantitative estimates using the SEM (assuming that the XRD results are correct).

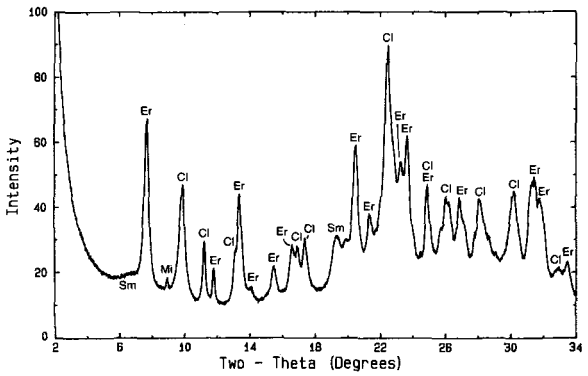

Figure 7. X-ray powder diffraction pattern (CuKα) of fracture-filling material from Yucca Mountain sample UE-25a#1 at 395.1-m depth. Er = erionite, Cl = clinoptilolite, Sm = smectite, and Mi = mica.

Yucca Mountain samples. Of the numerous Yucca Mountain samples analyzed, erionite was identified positively in only four. In samples J-12, 189.0–192-m and USW G-4, 400.51-m depth (sample designations refer to the drill core depth or depth range from given drill holes), erionite was detected in amounts less than 1 wt. % in the whole rock. A fracture from drill hole USW GU-3 at 362.5–362.6-m depth contained 0.35% erionite, and in a fourth sample (UE-25a#1, 395.1-m depth) erionite was a major component (Figure 7, 45 ± 10% erionite, 45 ± 10% clinoptilolite, 10 ± 5% smectite, and a trace of mica) filling a fracture. All four of these erionite occurrences are above the water table in clay- and zeolite-rich altered zones at the top of vitrophyres. At least three of them occur above the lower vitrophyre of the Topopah Spring Member. The stratigraphy of drill hole J-12 is not well described, and the stratigraphic identity of the erionite-bearing zone in this hole is unknown.

Analyses of whole-rock samples 6.1 m above and 8.5 m below the UE-25a#1 fracture sample showed no detectable amounts of erionite, illustrating the isolated nature of the erionite distribution. Furthermore, nine neighboring fracture samples from the altered zone in the Topopah Spring lower vitrophyre in UE-25a#1, ranging from 16.5 m above to 20.1 m below and as

https://doi.org/10.1346/CCMN.1991.0390413 Published online by Cambridge University Press

close as 1.8 m to the erionite-containing fracture at 395.1-m depth, also showed no evidence of erionite.

Although other samples in the altered zones in these four drill holes did not contain erionite, the clay- and zeolite-rich horizons contained an unusual array of other zeolites, including clinoptilolite/heulandite, mordenite, phillipsite, chabazite, and stilbite (or stellerite) (e.g., Table 1 for drill hole UE-25a#1). Apart from clinoptilolite/heulandite and mordenite, none of these zeolites is common in other rocks at Yucca Mountain. The restricted nature of erionite and the variety of zeolites occurring over a small vertical distance within the altered zone in a variety of drill cores taken from Yucca Mountain suggest that unusual and variable conditions must have prevailed in these zones during zeolite formation.

Table 1. Alteration mineralogy adjacent to the lower vitrophyre of the Topopah Spring Member in drill hole UE-25a#1 at Yucca Mountain.

Depth (m)	Sm	Cl	Mo	Er	Ph
378.77–378.90		X	X		
381.70		X	X		
388.47	X	X			
388.92–388.99	X	X			
390.94	X	X			
395.08	X	X		X	
396.70–396.91	X	X			X
403.22–403.31	X	X	X		
408.28–408.34		X	X		
415.08–415.14	X	X	X		

Sm = smectite; Cl = clinoptilolite; Mo = mordenite; Er = erionite; Ph = phillipsite.

SUMMARY AND CONCLUSIONS

The results of this study demonstrate that even complex materials with low reference intensity ratios and strong reflections at low angles can be identified accurately at concentrations $\ll 1\%$ using X-ray powder diffraction. As with other methods of trace mineral analysis, great care must be taken to choose the correct sample and instrument parameters and the appropriate standards. Use of incident-beam Soller slits and sufficiently long count times are particularly important when quantifying erionite. These factors are considerably less important when quantifying materials such as quartz and cristobalite with high RIR values and major reflections $>20°2\theta$.

When quantifying low levels of erionite, any procedure that reduces background intensity in the 6–8°2θ (CuKα) range or minimizes overlap of extraneous peaks with the erionite 100 reflection will improve detection limits. Use of a sample cell with a helium atmosphere may assist in reduction of low-angle air scatter and thereby improve the detection of a small erionite 100 reflection. Solvation of smectite with ethylene glycol (with or without a helium atmosphere) significantly improves the detection of erionite. In general, however, for samples containing smectite, the absolute erionite detection limit will depend on the total smectite concentration. Given the range of minerals coexisting with erionite and present conventional X-ray powder diffraction instrument technology, the LLD for erionite using <12-hr scans is ~ 100 ppm if no interfering phases are present. It is between 250 and 700 ppm if phases such as clinoptilolite or smectite are present. Longer count times, higher-power X-ray sources, or position-sensitive detectors can improve the detection limits for erionite to <100 ppm. Detection of erionite $\leq$ the 250–700-ppm level with a SEM probably will be difficult. SEM detection will depend upon sample preparation procedures, the areal amount of sample examined, and the nature of the erionite distribution in the solid sample. If erionite is detected using the SEM, quantification can probably be better achieved using X-ray powder diffraction. Detection of erionite below the 100-ppm level will probably be more successful using the transmission electron microscope (TEM), coupled with electron diffraction to provide unambiguous identification. However, precise quantification of erionite at these low concentrations using the TEM will be difficult, will depend on sample preparation techniques, and will require examination of large areas on the TEM scale.

Although erionite has been reported to be one of the most tumorigenic materials yet studied (Wagner *et al.*, 1985), its presence in Yucca Mountain tuffs will probably not pose a problem in the construction or operation of a radioactive waste repository. The altered zone in which erionite has been found at Yucca Mountain is below the potential repository horizon. Any excavation beneath the repository into the altered zone would require appropriate precautions. In addition, the amount of erionite potentially liberated to the biosphere by repository construction and operation should be negligible or nonexistent. This contrasts with the significant amounts of erionite occurring naturally at the surface in Nevada and surrounding states (Papke, 1972; Sheppard and Gude, 1980).

ACKNOWLEDGMENTS

This work began as a result of discussions with F. A. Mumpton. We are grateful to him for providing samples and for valuable comments on the manuscript. We also gratefully acknowledge G. D. Guthrie for information on the health effects of erionite. G. D. Guthrie, D. T. Vaniman, and R. A. Sheppard offered constructive comments on the manuscript. B. Carlos and D. E. Broxton provided samples of fracture fillings from Yucca Mountain. This work was supported by the Yucca Mountain Site Characterization Project Office as part of the Civilian Radioactive Waste Management Program.

REFERENCES

Bariş, Y. I., Özemsi, M., Kerse, I., Özen, E., Şahin, A., Kolaçan, B., and Ogankulu, M. (1975) An outbreak of pleural mesothelioma in the village of Karain/Ürgüp—Anatolia: *Kanser* **5,** 1–14.

Baris, I., Simonato, L., Artvinli, M., Pooley, F., Saracci, R., Skidmore, J., and Wagner, C. (1987) Epidemiological and environmental evidence of the health effects of exposure to erionite fibres: A four-year study in the Cappadocian region of Turkey: *Int. J. Cancer* **39,** 10–17.

Bish, D. L. (1984) Effects of exchangeable cation composition on the thermal expansion/contraction of clinoptilolite: *Clays & Clay Minerals* **32,** 444–452.

Bish, D. L. and Chipera, S. J. (1989a) Revised mineralogic summary of Yucca Mountain, Nevada: *Los Alamos Nat. Lab. Rept.* **LA-11497-MS,** 68 pp.

Bish, D. L. and Chipera, S. J. (1989b) Comparison of a solid-state Si detector to a conventional scintillation detector-monochromator system in X-ray powder diffractometry: *Powder Diffraction* **4,** 137–143.

Broxton, D. E., Bish, D. L., and Warren, R. G. (1987) Distribution and chemistry of diagenetic minerals at Yucca Mountain, Nye County, Nevada: *Clays & Clay Minerals* **35,** 89–110.

Carlos, B. A. (1985) Minerals in fractures of the unsaturated zone from drill core USW G-4, Yucca Mountain, Nye County, Nevada: *Los Alamos Nat. Lab. Rept.* **LA-10415-MS,** 55 pp.

Carter, J. R., Hatcher, M. T., and Di Carlo, L. (1987) Quantitative analysis of quartz and cristobalite in bentonite clay based products by X-ray diffraction: *Anal. Chem.* **59,** 513–519.

Chipera, S. J. and Bish, D. L. (1989) The occurrence and distribution of erionite at Yucca Mountain, Nevada: *Los Alamos Nat. Lab. Rept.* **LA-11663-MS,** 20 pp.

Chung, F. H. (1974) Quantitative interpretation of X-ray diffraction patterns of mixtures. II. Adiabatic principle of X-ray diffraction analysis of mixtures: *J. Appl. Crystallogr.* **7,** 526–531.

Coffin, D. L., Peters, S. E., Palekar, L. D., and Stahel, E. P. (1989a) A study of the biological activity of erionite in relation to its chemical and structural characteristics: in *Proceedings of Biological Interaction of Inhaled Mineral Fibers and Cigarette Smoke,* A. P. Wehner, ed., Battelle Press, Columbus, Ohio, 313–323.

Coffin, D. L., Palekar, L. D., Cook, P. M., and Creason, J. P. (1989b) Comparison of mesothelioma induction in rats by asbestos and nonasbestos mineral fibers: Possible correlation with human exposure data: in *Proceedings of Biological Interaction of Inhaled Mineral Fibers and Cigarette Smoke,* A. P. Wehner, ed., Battelle Press, Columbus, Ohio, 347–354.

Davis, B. L. (1988) The estimation of limits of detection in RIM quantitative X-ray diffraction analysis: *Adv. X-ray Analysis* **31,** 317–323.

Deffeyes, K. S. (1959) Erionite from Cenozoic tuffaceous sediments, central Nevada: *Amer. Mineral.* **44,** 501--509.

Klug, H. P. and Alexander, L. E. (1974) *X-ray Diffraction Procedures for Polycrystalline and Amorphous Materials:* Wiley, New York, 524–525.

Mumpton, F. A. (1979) A reconnaissance study of the association of zeolites with mesothelioma occurrences in central Turkey: *U.S. Geol. Surv. Open-File Rept.* **79-954,** 55 pp.

Palekar, L. D., Eyre, J. F., and Coffin, D. L. (1989) Chromosomal changes associated with tumorigenic mineral fibers: in *Proceedings of Biological Interaction of Inhaled Mineral Fibers and Cigarette Smoke,* A. P. Wehner, ed., Battelle Press, Columbus, Ohio, 355–372.

Papke, K. G. (1972) Erionite and other associated zeolites in Nevada: *Nevada Bur. Mines & Geol. Bull.* **79,** 32 pp.

Puledda, S. and Marconi, A. (1989) Quantitative X-ray diffraction analysis of four types of amphibolic asbestos by the silver membrane filter method: *Intern. J. Environ. Anal. Chem.* **36,** 209–220.

Rohl, A. N., Langer, A. M., Moncure, G., Selikoff, I. J., and Fischbein, A. (1982) Endemic pleural disease associated with exposure to mixed fibrous dust in Turkey: *Science* **216,** 518–520.

Sèbastien, P., Bignon, J., Barris, Y. I., Awad, L., and Petit, G. (1984) Ferruginous bodies in sputum as an indication of exposure to airborne mineral fibers in the mesothelioma villages of Cappadocia: *Arch. Environ. Health* **39,** 18–23.

Sheppard, R. A. and Gude, A. J., 3rd (1980) Diagenetic fluorite in the Eastgate zeolite deposit, Churchill County, Nevada: *U.S. Geol. Surv. Open-File Rept.* **80-506,** 8 pp.

Simonato, L., Baris, R., Saracci, R., Skidmore, J., and Winkelmann, R. (1989) Relation of environmental exposure to erionite fibres to risk of respiratory cancer: in *Non-occupational Exposure to Mineral Fibres,* J. Bignon, J. Peto, and R. Saracci, eds., Intern. Agency for Research on Cancer, Lyon, France, 398–405.

Smith, D. K., Nichols, M. C., and Zolensky, M. E. (1982) POWD10. A FORTRAN IV program for calculating X-ray powder diffraction patterns—version 10: The Pennsylvania State University, University Park, Pennsylvania.

Suzuki, Y. and Kohyama, N. (1988) Carcinogenic and fibrogenic effects of erionite, mordenite, and synthetic zeolite 4A: in *Occurrence, Properties, and Utilization of Natural Zeolites,* D. Kallo and H. S. Sherry, eds., Akademiai Kiado, Budapest, 829–840.

Wagner, J. C., Skidmore, J. W., Hill, R. J., and Griffiths, D. M. (1985) Erionite exposure and mesotheliomas in rats: *Br. J. Cancer* **51,** 727–730.

(*Received 14 January 1991; accepted 12 March 1991; Ms. 2065*)